Role of Electronic Excitations in Ground-State-Forbidden Inelastic Collisions Between Ultracold Atoms and Ions

Scott T. Sullivan, Wade G. Rellergert, Svetlana Kotochigova, and Eric R. Hudson

Phys. Rev. Lett. **109**, 223002 — Published 27 November 2012

DOI: 10.1103/PhysRevLett.109.223002

The role of electronic excitation in ground-state forbidden inelastic collisions between ultracold atoms and ions

Scott T. Sullivan,[1] Wade G. Rellergert,[1] Svetlana Kotochigova,[2] and Eric R. Hudson[1]

[1]*Department of Physics and Astronomy, University of California, Los Angeles, California 90095, USA*
[2]*Department of Physics, Temple University, Philadelphia, Pennsylvania 19122, USA*

(Dated: September 20, 2012)

The role of electronic excitation in inelastic collisions between ultracold Ca atoms and Ba^+ ions, confined in a hybrid trap, is studied for the first time. Unlike previous investigations, this system is energetically precluded from undergoing inelastic collisions in its ground state, allowing a relatively simple experimental determination and interpretation of the influence of electronic excitation. It is found that while the electronic state of the ion can critically influence the inelastic collision rate, the polarizability mismatch of the neutral atom electronic states suppresses short-range collisions, and thus inelastic processes, involving electronically excited neutral atoms. As a result of these features, it is experimentally demonstrated that it is possible to mitigate inelastic collision loss mechanisms in these systems, marking an important step toward long-lived hybrid atom-ion devices.

PACS numbers:

Since the inception of laser-cooling, a chief focus of atomic physics has been the development of techniques for the production and study of ultracold matter – an endeavor that is centered on facilitating full control over matter at the quantum level. This work has been quite successful, enabling many long-sought-after goals, such as quantum degenerate gases [1, 2], quantum simulation [3], quantum information [4], and precision measurement of fundamental physics [5, 6]. To gain this control, however, most ultracold matter production techniques rely on the scattering of a large number of photons from the system under study, potentially leading to a large degree of electronic excitation. Thus, the atom or molecule being cooled can be in a peculiar state: its external motion may be characterized by a temperature close to absolute zero, but its internal electronic degree of freedom may be characterized by a temperature approaching infinity. While this non-thermal distribution of electronic states has some notable important consequences for ultracold atoms [7], most of its effects, such as photochemical reactions [8–10], are largely ignored as they occur at rates that have relatively little effect on the system. However, as the field now moves towards producing more complex systems at ultracold temperatures, *e.g.* molecules [11] and hybrid systems [12, 13], the effect of these light-assisted processes must be reevaluated as their rates may be much larger due to, among other things, an increased density of accessible product states and longer range interactions. Thus, there is presently a need to better understand the role of electronic excitation in inelastic processes, such as chemical reactions, at ultracold temperatures to enable the next generation of experiments.

Interestingly, the rapidly emerging field of hybrid atom-ion systems offers a unique opportunity to study ultracold collisions [14–17]. Like in all-neutral systems of traditional atomic physics, the co-trapped species can collide at short-enough range for reactions to proceed; but, unlike all-neutral systems it is possible to maintain a product of the reaction in the trap, since ion trap depths are large relative to the typical exothermic energy release. Already, such hybrid systems have been used to measure several important ion-neutral chemical reactions [13–16], culminating in the recent observation of molecular ion reaction products [17].

Here, we use a hybrid atom-ion MOTION trap system [16, 17] to study chemical reactions between ultracold ^{40}Ca atoms and $^{138}Ba^+$ ions. Unlike all previous studies, inelastic collisions between ground-state atoms and ions are energetically forbidden in the $^{40}Ca + {}^{138}Ba^+$ system and can thus only occur if at least one species is electronically excited. As a result, this system is relatively simple to interpret and allows a straightforward examination of the role of electronic excitation. In what follows, we discuss how optical coherence and trap dynamics can critically affect the observed atom-ion chemical reaction rate when electronic excitation is involved, and present experimental results detailing the observed chemical reaction pathways and the average radiative association branching ratio for formation of $CaBa^+$ molecular ions. We also present relativistic *ab initio* molecular structure calculations, which further illuminate the excited state entrance channels, as well as provide guidance for future experiments. We additionally present the first detailed experimental investigation of the importance of neutral atom excitation and conclude with a demonstration that it is possible, with reasonable experimental parameters, to avoid the large chemical reaction rates seen in other hybrid atom-ion systems, marking a crucial step towards the next generation of hybrid atom-ion devices.

The apparatus used in this work is similar to that described in Ref. [16]. Briefly, $^{138}Ba^+$ ions ($N_{\mathrm{ion}} \sim 1000$ ions) are loaded into a linear radio-frequency (rf) quadrupole trap via laser ablation of a $BaCl_2$ target [18] and cooled with colinear laser beams. In the same region,

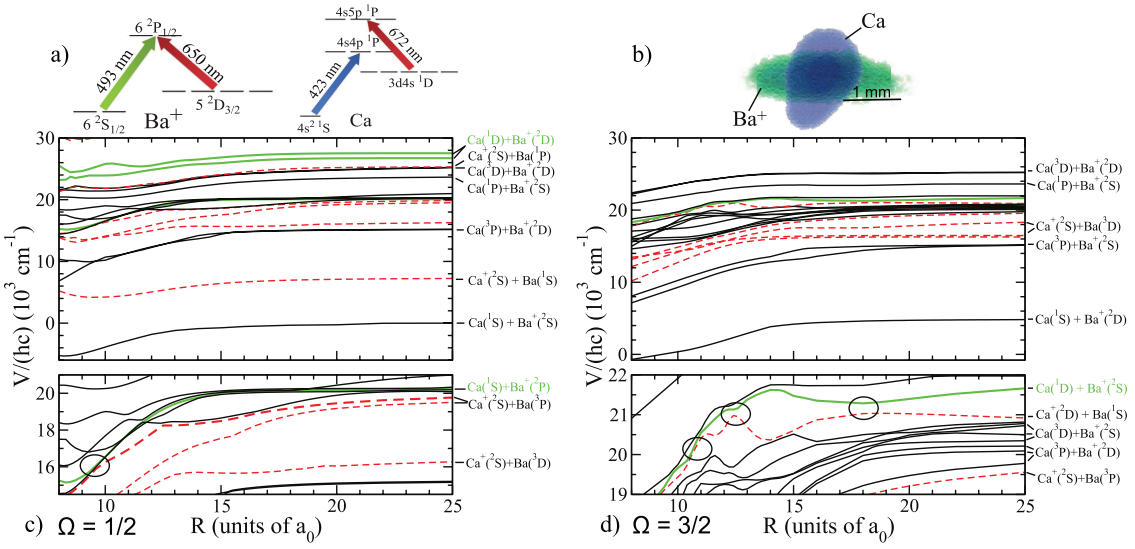

FIG. 1: a) Ba^+ and Ca relevant energies levels and laser cooling schemes. b) Fluorescence images of Ca MOT and Ba^+ ion cloud. c) and d) Molecular potentials of the $\Omega=\frac{1}{2}, \frac{3}{2}$ excited states of the $CaBa^+$ molecule, respectively, as a function of interatomic separation R. The bottom panels show higher detail for potentials near 20×10^3 cm^{-1} above the $Ca^+(^2S)$+$Ba(^1D)$ dissociation limit. Entrance and exit channels, as defined in the text, dissociate to green and red potentials, respectively.

ultracold Ca atoms ($N_{\rm MOT} \sim 3\times10^6$ atoms, $\rho_{\rm MOT} \sim 5\times10^9$ cm^{-3}) are produced and trapped in a magneto-optical trap (MOT). (See Fig. 1(a) for the ion and atom electronic energy levels and cooling laser scheme, denoted by arrows.) Two nearly-orthogonal cameras allow for a 3-dimensional reconstruction of both the Ca MOT and the laser-cooled ion cloud, and are used to quantify the degree of overlap between the Ca atoms and $^{138}Ba^+$ ions, as shown in Fig. 1(b). Using the same approach as Ref. [16], the laser-induced 493 nm fluorescence monitors the $^{138}Ba^+$ ion population, which is observed to decay in the presence of the Ca MOT due to charge exchange chemical reactions ($Ca+Ba^+ \rightarrow Ca^+ + Ba$, $CaBa^+ + \gamma$), allowing a direct measurement of the total inelastic collision (charge transfer) rate Γ.

In this experiment, the atom-ion collision energies are primarily set by the coherent, driven motion of the ion due to the rf trapping potential (i.e. the micromotion) since the Ca MOT temperature ($T \simeq 4$ mK) and the Doppler-cooling temperature limit of the Ba^+ ions ($T \simeq 0.5$ mK) are both lower than the typical, position dependent, energy of micromotion in the ion cloud ($\frac{E_\mu}{k_B} \sim$10 mK-10 K). At these low collision energies, chemical reaction dynamics are primarily determined by the relative energies of the entrance and exit reaction channels, shown in black and red, respectively, in Fig. 1(c,d). Because the ionization potential of Ca (6.1 eV) is significantly larger than that of Ba (5.2 eV), charge exchange reactions between the Ca 4^1S- and Ba^+ 6^2S- or 5^2D-electronic states are energetically precluded. As a result, inelastic collision between Ba^+ and Ca can only occur if the atom, the ion, or both are electronically excited. Of the ten energetically allowed entrance channels populated in this experiment, the six involving the short-lived Ca P-states do not contribute to the observed reaction rate. Because the Ca 4^1S-, 4^1P- and 5^1P-states have very different atomic polarizabilties [19] (163.0 a.u., 55.3 a.u., and >1000 a.u., respectively), during the collision the strong monopole field of the ion alters the atomic transition frequency such that the Ca MOT lasers are shifted far from resonance for atom-ion separations of many hundred Bohr radii, a_o. Thus, though a collision leading to reaction may begin with a Ca atom in a P-state, by the time the atom and ion are close enough to react ($< 10\, a_o$), the Ca atom has radiatively decayed from the P-state. We note similar effects are discussed in Ref. [14, 20, 21], were observed in Ref. [16], and are confirmed by the data presented here. This effect appears general and it is likely that short-lived excitations of ultracold atoms can be ignored in future experiments involving reactions of ultracold atoms and ions. (This effect is particularly beneficial to techniques for sympathetic cooling of molecular ions by ultracold atoms [22], as it significantly relaxes the experimental constraints.) Interestingly, a similar argument cannot be made for short-lived, excited states of ions. Because excitation of the ion only changes the long-range dispersion coefficient, e.g. C_6, the ion cooling lasers are not shifted out of resonance until relatively small atom-ion separations. Thus, while these chemical reactions are suppressed, it is nonetheless possible for them to occur between atoms and excited state ions.

With these considerations, it is clear that the reactions proceed from the energetically allowed entrance channels involving 4^1S- or 3^1D-state Ca atoms and 6^2S-, 6^2P-, or

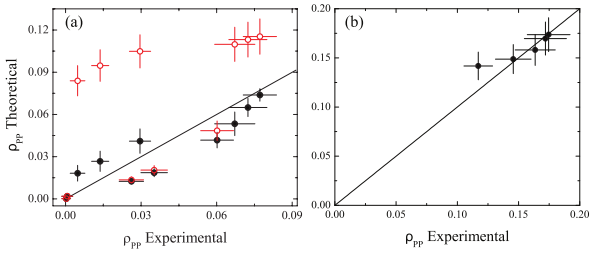

FIG. 2: Panel (a): experimentally determined excitation fraction in Ba^+ versus theoretical predictions of the quantum Liouville (•) and rate equation (○) treatment. Panel (b): experimentally determined excitation fraction in Ca versus predictions of a 4-level rate equation model. In both panels the solid line has a unit slope, representing ideal agreement.

5^2D-state Ba^+ ions, highlighted in green in Fig. 1(c-d). While the charge exchange rate constant for each of the four distinct pathways depends sensitively on the details of the $CaBa^+$ molecular structure, they can nevertheless be probed by varying the excited state populations of the atoms and ions while recording the total reaction rate. Experimentally, this is accomplished by varying the intensities of the atom and ion cooling lasers. With known experimental parameters it is then possible to calculate the relative population of each atom and ion electronic state (we denote the population fraction of the specie X in the electronic state i by its diagonal density matrix element ρ_{ii}^X), and extract the contribution of each reaction channel to the total measured reaction rate given by $\Gamma = \rho_{\rm MOT}\langle\sigma v\rangle = \rho_{\rm MOT} k_{\rm Total} = \rho_{\rm MOT}\sum_{i,j}\rho_{ii}^{Ba}\rho_{jj}^{Ca}k_{i,j}$, where $k_{i,j}$ is the rate constant for Ba^+ in electronic state i immersed in a pure sample of Ca in electronic state j.

The calculation of the Ba^+ electronic state populations is complicated by optical coherence effects and the quadrupole magnetic field of the MOTION trap, whose direction and strength vary in a non-trivial way. Therefore, we determine the Ba^+ electronic state populations by solving the steady-state quantum Liouville equation for an eight-level optical Bloch Hamiltonian [23] and spatially averaging the result over the ion cloud. To confirm the accuracy of this calculation, we directly measure the Ba^+ $6^2P_{1/2}$ state fraction via calibrated fluorescence and ion detection, as shown in Fig. 2(a) along with the prediction of a standard rate equation model for comparison. Similarly, a first principles calculation of the electronic state populations of atoms in a MOT environment is a well-known open problem and various phenomenological models have been proposed [24, 25]. Therefore, we directly measure the Ca 4^1P-state excitation fraction to determine the appropriate model for calculation of the Ca population fractions. As shown in Fig. 2(b), we find good agreement with a standard four-level rate equation model [10], a likely consequence of the lack of hyperfine structure in ^{40}Ca.

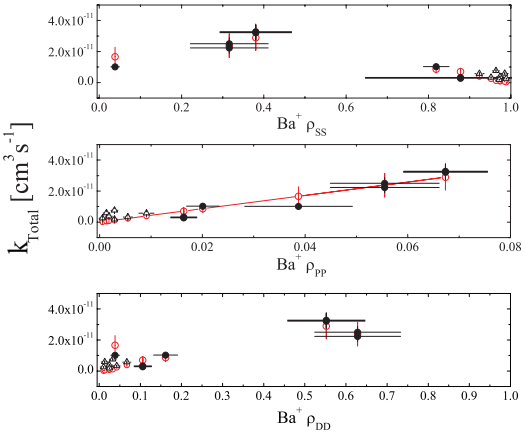

FIG. 3: Measured rate constant as a function of Ba^+ population fractions. Experimental result in black. Best fit $(\{k_{ps}, k_{sd}, k_{pd}, k_{dd}\}=\{4.2 \pm 1.9, \leq 3, \leq 20, \leq 7\} \times 10^{-10}$ cm^3 s^{-1}) to the four entrance channel model shown as open red circles (○).For these measurements, Ca population fractions were fixed at $\rho_{ss}^{Ca} \sim 0.75$, $\rho_{pp}^{Ca} \sim 0.20$, $\rho_{dd}^{Ca} \sim 0.05$.

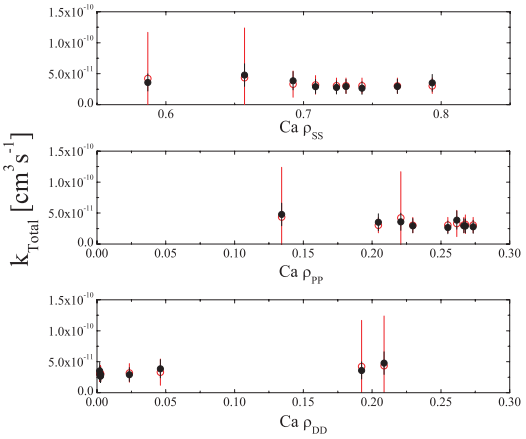

FIG. 4: Measured rate constant as a function of Ca population fractions. Experimental result in black. Best fit $(\{k_{ps}, k_{sd}, k_{pd}, k_{dd}\}=\{4.2 \pm 1.9, \leq 3, \leq 20, \leq 7\} \times 10^{-10}$ cm^3 s^{-1}) to the four entrance channel model shown as open red circles(○). For these measurements, the Ba^+ population fractions were fixed at $\rho_{ss}^{Ba} \sim 0.4$, $\rho_{pp}^{Ba} \sim 0.1$, $\rho_{dd}^{Ba} \sim 0.5$.

With these tools in place, we vary the laser intensities, calculate the resulting excitation fractions, and record the total inelastic rate constant. The resulting measurements, plotted as a function of ion and atom excitation fraction, are shown in Figs. 3 and 4, respectively.

As a function of Ba^+ excitation, the most obvious feature is a linear trend of increasing reactivity with increasing ρ_{pp}^{Ba}. In addition, the reaction rate constant diminishes at both extremes of the Ba^+ S-state, ρ_{ss}^{Ba}, and D-state, ρ_{dd}^{Ba}, population fraction. Taken together, these features indicate that the primary reaction channel involves the Ba^+ ion P-state, since a comparable S- or D-state contribution would result in measurable rate

constants in the limit of unit occupation of the S- or D-state. Also shown in Fig. 3, as open triangles, are several measurements at low excitation fractions ($< 1\%$). While these points agree with the rest of the data, they are not included in the final analysis to avoid possible systematic inaccuracies due to higher secular energies.

As shown in Fig. 4, the rate constant exhibits no detectable variation over the experimentally accessible Ca excitation range. Neither the Ca 5^1P-state nor the 4^1P-state are expected to contribute to the rate constant shown here, the former due to a negligible population and the latter due the aforementioned radiative suppression effect. As a result only the Ca S- and D-states contribute to the observed reaction rate, thus we conclude that the lack of a trend in Fig. 4 is an indication of similar reaction rates for the atomic S- and D-states with Ba^+.

To extract channel-specific reaction rate constants from these data, we quantify the total reaction rate constant in terms of the excited state fractions of both Ba^+ and Ca as: $k_{\mathrm{Total}} = \rho_{pp}^{Ba}\rho_{ss}^{*Ca}k_{ps} + \rho_{ss}^{Ba}\rho_{dd}^{Ca}k_{sd} + \rho_{dd}^{Ba}\rho_{dd}^{Ca}k_{dd} + \rho_{pp}^{Ba}\rho_{dd}^{Ca}k_{pd}$. By accounting for the conservation of probability ($\rho_{ss} = 1 - \rho_{pp} - \rho_{dd}$) and the fact that Ca atoms in the P-state radiatively decay to the S-state before the atom and ion are close enough to react ($\rho_{ss}^{*Ca} = \rho_{ss}^{Ca} + \rho_{pp}^{Ca}$), the totality of the data in Fig. 3 and Fig. 4 is subject to a multi-parameter fit along the manifold $\{\rho_{pp}^{Ba}, \rho_{dd}^{Ba}, \rho_{dd}^{Ca}\}$ to determine the contribution of each reaction pathway to the total rate constant. From this fit, the reaction rate constant of the primary entrance channel, $Ba^+(6^2P_{1/2}) + Ca(4^1S)$, is found to be $k_{ps} = 4.2(1.9) \times 10^{-10}$ cm^3 s^{-1}, while the best fit for the rate constant of the only channel out of the Ba^+ ground state, $Ba^+(6^2S_{1/2}) + Ca(3^1D)$ is constrained to be $\leq 3 \times 10^{-10}$ cm^3 s^{-1}. Because the remaining two entrance channels, $Ba^+(6^2P_{1/2}) + Ca(3^1D)$ and $Ba^+(5^2D_{3/2}) + Ca(2^1D)$, require simultaneous excitation of the atom and ion, our experiment is relatively insensitive to them and we set upper limits on them of $k_{pd} \leq 2 \times 10^{-9}$ cm^3 s^{-1} and $k_{dd} \leq 7 \times 10^{-10}$ cm^3 s^{-1}. To show the quality of agreement between the best fit and the results, we plot a data point generated from the fit corresponding to each experimental condition (open circles) in Figs. 3 and 4. In addition to this fit, using the method described in Ref. [16], we measure the molecular ion product branching ratio to be ~ 0.1. Future measurements, using time-of-flight detection as in Ref.[26], are planned to further constrain the branching ratio.

To illuminate the charge exchange mechanisms responsible for the individual reaction pathways, we performed *ab initio* calculations of the $CaBa^+$ potentials, with total body-fixed angular momentum of $\Omega = (\frac{1}{2}, \frac{3}{2})$, using a relativistic multi-reference restricted active space configuration-interaction method [27]. Spin-orbit effects are large in $CaBa^+$ and a relativistic calculation is required. The resulting Born-Oppenheimer potentials for the ground and first-excited state of $CaBa^+$ are shown in Fig. 1(c-d), and assigned by their atomic dissociation limit. The bottom panels of Fig. 1(c-d) show a higher resolution view of the closely spaced potentials above 20×10^3 cm^{-1}. Both panels reveal that there are strong interactions and avoided crossings between neighboring excited potentials. Potentials dissociating to energies $> 27 \times 10^3$ cm^{-1} are not shown, as the exceedingly high level density makes it impossible to resolve the avoided crossings with our calculation.

In principle, a coupled-channels calculation that includes the mixings between these potentials due to radial non-adiabatic coupling and spontaneous emission, like that performed in Ref. [16], can be used to calculate the non-radiative, radiative, and radiative association charge exchange reaction rate constants for each entrance channel; however, due to the high level density in the excited $CaBa^+$ molecule, this calculation is extremely technically demanding and falls outside the scope of this work. Nonetheless, the basic mechanisms of each charge exchange pathway can be qualitatively inferred from the calculated structure of its entrance channel molecular potential. For example, the experimentally dominant entrance channel, $Ca(4^1S) + Ba^+(6^2P_{1/2})$, exhibits strong interactions with several potentials as well as a narrowly-avoided crossing with a molecular potential dissociating to the $Ca^+(4^2S) + Ba(6^3P)$ exit channel. The second most experimentally reactive entrance channel, $Ca(3^1D) + Ba^+(6^2S_{1/2})$, also shows several strong avoided crossings with the $Ca^+(3^2D) + Ba(6^1S)$ exit channel. Strong, narrowly-avoided crossings facilitate non-adiabatic, non-radiative charge transfer, the likely mechanism for the aforementioned channels. By similar reasoning, it is expected that the $Ca(3^1D) + Ba^+(5^2D)$ entrance channel would be relatively inefficient for charge exchange reactions since low energy scattering events do not experience an avoided crossing nor do they couple well to states accessible via spontaneous emission due to poor Franck-Condon overlap. The remaining $Ca(3^1D) + Ba^+(6^2P_{1/2})$ entrance channel resides in a host of densely packed levels, which prevents our *ab initio* calculation from providing reliable results and suggests that non-radiative and radiative chemical reactions could proceed very quickly from these states, a result that is consistent with the limit set for this channel by our measurement.

Finally, despite the fact that the rate constants measured here are large by atomic physics standards, roughly a third of the rate attained when assuming all collisions that cross the angular momentum barrier have a unit probability of being inelastic (i.e. the Langevin rate), with proper engineering of the atomic and ionic excited state populations, their effects can be mitigated. By using sufficient repumping laser powers to maintain a negligible Ca D-state fraction and using the minimum ion laser cooling power necessary to achieve Doppler-limited cooling, we have observed Ba^+ ion lifetimes in excess of several minutes in the presence of the MOT.

In summary, we have experimentally studied chemical reactions in a hybrid atom-ion system, where only electronically excited states are permitted to react. The observed reaction dynamics are qualitatively different than what is observed in systems where ground-state reactions are equally important [16]. The measured reaction rate constant is found to be an appreciable fraction of the Langevin rate, similar to results found in other experiments involving excitation [14, 17, 28], and is mostlikely due to non-radiative charge transfer occurring at narrowly-avoided crossings in at least two of the entrance channels. We have also demonstrated that, with a judicious choice of atomic species and degree of electronic excitation, it is possible to engineer experiments where the cold reactive species can co-exist for several minutes. From these results it is clear that a new generation of hybrid-atom ion devices, capable of the long coherence times needed for proposed hybrid atom-ion systems [22, 29–33] is in reach.

This work was supported by NSF grant No. PHY-1005453, ARO grant No. W911NF-10-1-0505 and AFOSR grant No. FA 9550-11-1-0243.

[1] J. Ensher et al., Science **269**, 198 (1995).
[2] D. Jin and B. Demarco, Science **285**, 1703 (1999).
[3] I. Buluta and F. Nori, Science **326**, 108 (2009).
[4] T. D. Ladd et al., Nature **464**, 45 (2010).
[5] S. Bennett and C. Wieman, Phys. Rev. Lett. **82**, 2484 (1999).
[6] T. Rosenband et al., Science **319**, 1808 (2008).
[7] D. Sesko et al., Phys. Rev. Lett. **63**, 961 (1989).
[8] P. Gould et al., Phys. Rev. Lett. **60**, 788 (1988).
[9] P. Lett et al., Phys. Rev. Lett. **67**, 2139 (1991).
[10] S. T. Sullivan et al., Phys. Chem. Chem. Phys. **13**, 18859 (2011).
[11] E. S. Shuman, J. Barry, and D. DeMille, Nature **467**, 820 (2010).
[12] C. Zipkes et al., Nature **464**, 388 (2010).
[13] S. Schmid, A. Harter, and J. H. Denschlag, Phys. Rev. Lett. **105**, 133202 (2010).
[14] A. Grier et al., Phys. Rev. Lett. **102**, 223201 (2009).
[15] C. Zipkes et al., Phys. Rev. Lett. **105**, 133201 (2010).
[16] W. G. Rellergert et al., Phys. Rev. Lett. **107**, 243201 (2011).
[17] F. H. J. Hall et al., Phys. Rev. Lett. **107**, 243202 (2011).
[18] K. Chen et al., Phys. Rev. A **83**, 030501(R) (2011).
[19] M. Mohammadou, C. Tendero, and M. Rérat, Chem. Phys. Lett. **343**, 397 (2001).
[20] Y. B. Band and P. Julienne, Phys. Rev. A **46**, 330 (1992).
[21] C. D. Wallace et al., Phys. Rev. Lett. **74**, 1087 (1995).
[22] E. R. Hudson, Phys. Rev. A **79**, 061407 (2009).
[23] S. Stenholm, *Foundations of Laser Spectroscopy* (Dover Publications, 2005).
[24] M. Shah et al., Phys. Rev. A **75**, 053418 (2007).
[25] J. Javanainen, J. Opt. Soc. Am. B **10**, 572 (1993).
[26] S. J. Schowalter et al., Rev. Sci. Instrum. **83**, 043103 (2012).
[27] S. Kotochigova and E. Tiesinga, J. Chem. Phys. **123**, 174304 (2005).
[28] L. Ratschbacher et al., Nat Phys **8**, 649 (2012).
[29] C. Schneider et al., Nature Photon. **4**, 772 (2010).
[30] A. P. Daley, O. P. Fedichev, and P. Zoller, Phys. Rev. A **69**, 022306 (2004).
[31] D. Schuster et al., Phys. Rev. A **83**, 012311 (2011).
[32] R. Côté, Phys. Rev. Lett. **85**, 5316 (2000).
[33] W. W. Smith, O. P. Makarov, and J. Lin, J. Mod. Opt. **52**, 2253 (2005).